Universal strangeness production and size fluctuactions in small and large systems

P. Castorina
Dipartimento di Fisica ed Astronomia
Università di Catania-Italy
In collaboration with M.Floris, S.Plumari, H.Satz

EPS – High Energy Conference

VENEZIA

5 - 12 July 2017

Enhanced production of multi-strange hadrons in high-multiplicity proton-proton collisions

ALICE Collaboration **Nature Phys. 13 (2017) 535-539**

observation of strangeness enhancement in high-multiplicity pp collisions. We find that the integrated yields of strange and multi-strange particles relative to pions increases significantly with the event charged-particle multiplicity. The measurements are in remarkable agreement with p–Pb collision results [10, 11] indicating that the phenomenon is related to the final system created in the collision. In high-multiplicity events strangeness production reaches values similar to those observed in Pb–Pb collisions, where a QGP is formed.

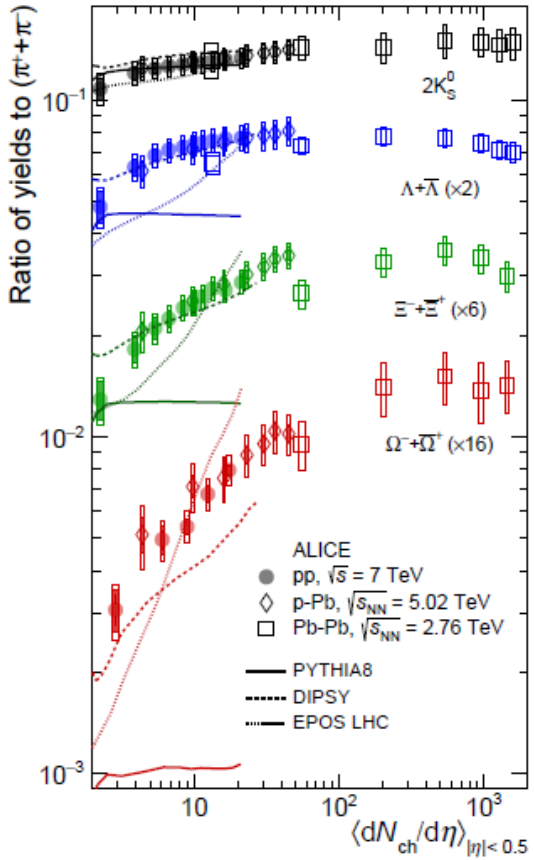

observation of strangeness enhancement in high-multiplicity pp collisions. We find that the integrated yields of strange and multi-strange particles relative to pions increases significantly with the event charged-particle multiplicity. The measurements are in remarkable agreement with p–Pb collision results [10, 11] indicating that the phenomenon is related to the final system created in the collision. In high-multiplicity events strangeness production reaches values similar to those observed in Pb–Pb collisions, where a QGP is formed.

Strangeness enhancement in pp at large energy : unexpected result

Almost…

Predicted in P.C and H.Satz **Strangeness Production in AA and pp Collisions** 1601.01454

P.C.,S.Plumari and H.Satz

Universal Strangeness Production in Hadronic and Nuclear Collisions 1603.06529

What is the effect of QGP formation on strange hadron production in high energy collisions?

Muller, Rafelski 1982

Relative Hadron Abundences in High Energy Collisions

Ideal gas of hadrons and resonances,
at temperature T, baryochemical potential μ.

In elementary collisions (pp, e^+e^-) up to RHIC energy and in nuclear collisions up to SPS energies:
overprediction of strange hadron production.

strangeness suppression factor γ_s, with γ_s^ν for hadrons with $\nu = 0, 1, 2, 3$ strange quarks

Letessier, Rafelski, Tounsi 1994

Ideal gas of hadrons and resonances, at temperature T,
baryochemical potential μ, strangeness suppression γ_s,
gives excellent agreement for abundances at all energies,
all collision configurations (e^+e^-, pp, pA, AA)

For $\sqrt{s} \geq 10$ GeV, $T \simeq 160 \pm 10$ MeV, for pp and AA, independent of μ, in accord with the color deconfinement temperature $T_c = 155 \pm 10$ MeV from lattice QCD.

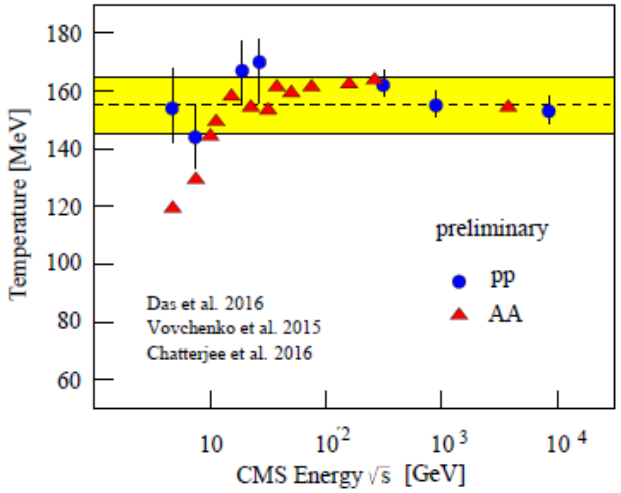

For AA below 10 GeV, increasing μ, decreasing T.

Strangeness suppression as function of $\sqrt{s}$ much stronger in pp than in AA:

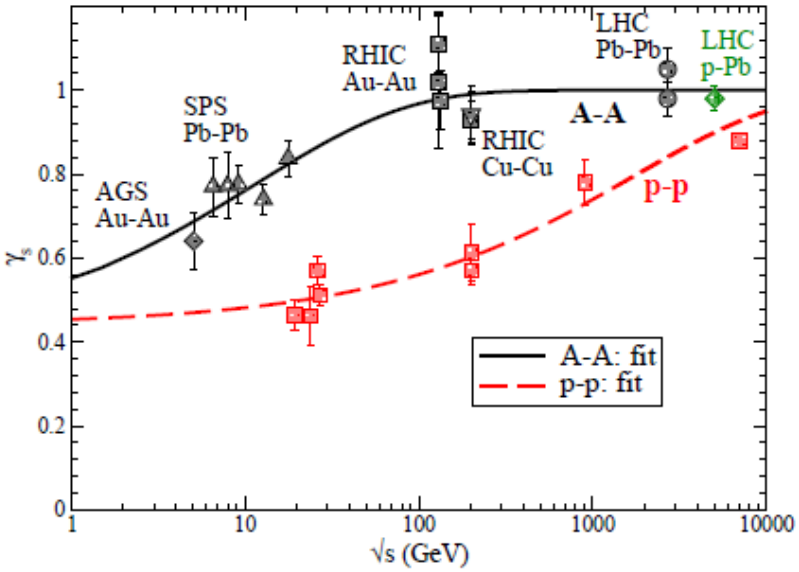

Becattini

fit curves for pp: $\gamma_s^p(s) = 1 - c_p \exp\left(-d_p s^{1/4}\right)$,
for AA: $\gamma_s^A(s) = 1 - c_A \exp\left(-d_A \sqrt{A\sqrt{s}}\right)$,
with $c_p = 0.5595;\ d_p = 0.0242;\quad c_A = 0.606,\ d_A = 0.0209.$

Is there a unified description of strangeness suppression?

Consider γ_s as function of pre-thermal or thermal variable.

Castorina, Plumari, HS 2016/2017

Average multiplicity

- 1d hydro (Bjorken) $\Rightarrow$ initial entropy density s_0

$$s_0\,\tau_0 \simeq \frac{1.5A^x}{\pi R_x^2}\left(\frac{dN_{ch}}{dy}\right)^x_{y=0}, \text{ with } x \sim pp, pA, AA,$$

multiplicities measured and fitted:

$$\left(\frac{dN}{dy}\right)^{AA}_{y=0} = a_A(\sqrt{s})^{0.3} + b_A$$

$$\left(\frac{dN}{dy}\right)^{pp}_{y=0} = a_p(\sqrt{s})^{0.22} + b_p$$

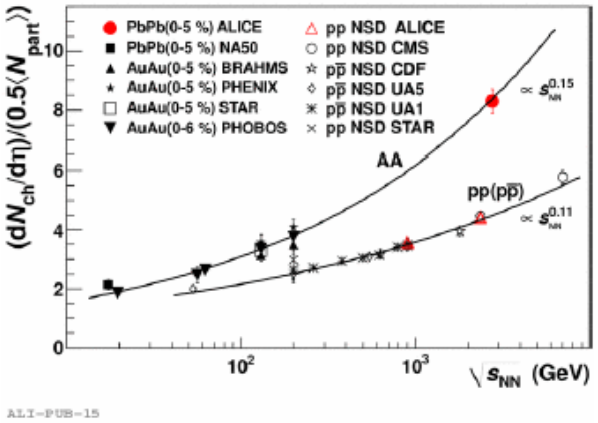

$a_A = 0.7613,\ b_A = 0.0534;\quad a_p = 0.797;\ b_p = 0.04123.$

Now have strangeness suppression factor $\gamma_s(s)$ and initial entropy density $s_0(s)$; eliminate s to get $\gamma_s(s_0)$:

Now have strangeness suppression factor $\gamma_s(s)$ and initial entropy density $s_0(s)$; eliminate s to get $\gamma_s(s_0)$:

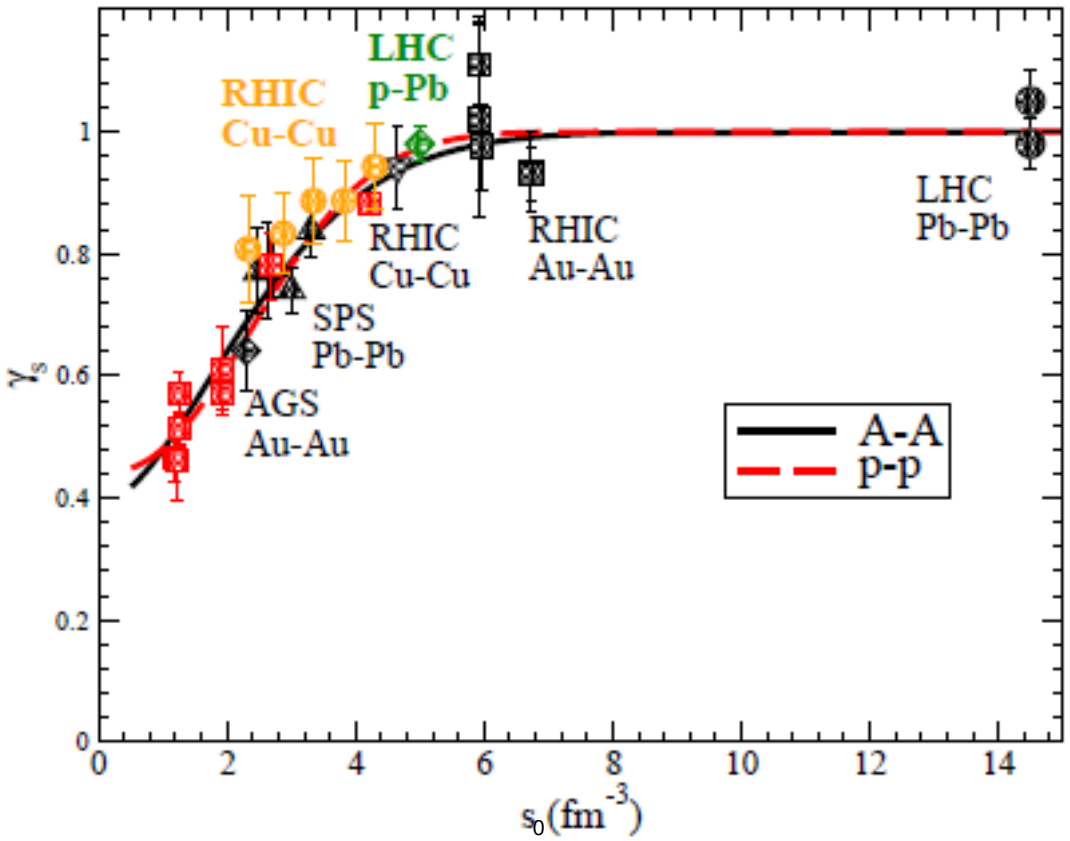

as function of the initial entropy density, the pp and AA curves for γ_s coincide, all data fall on the same curve:

universal strangeness suppression

in particular: $\gamma_s \longrightarrow 1$ also for high energy pp collisions

Castorina, HS 2016

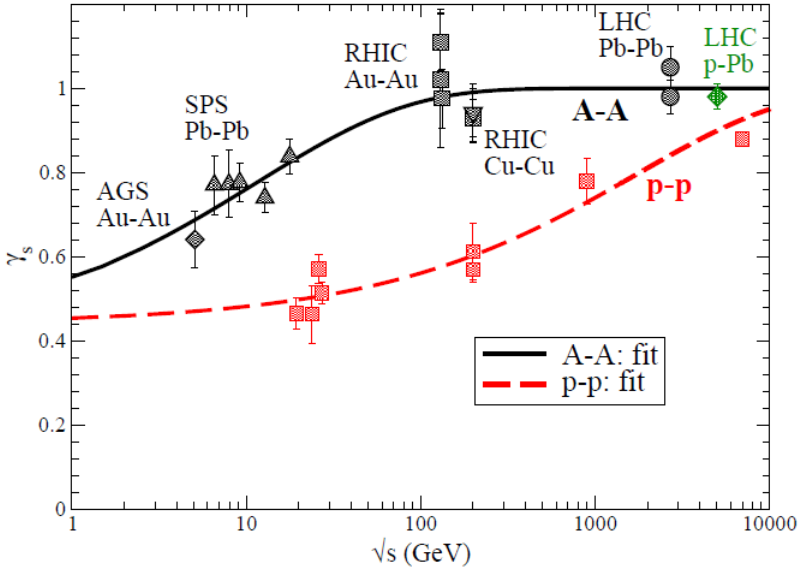

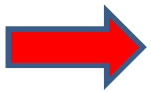

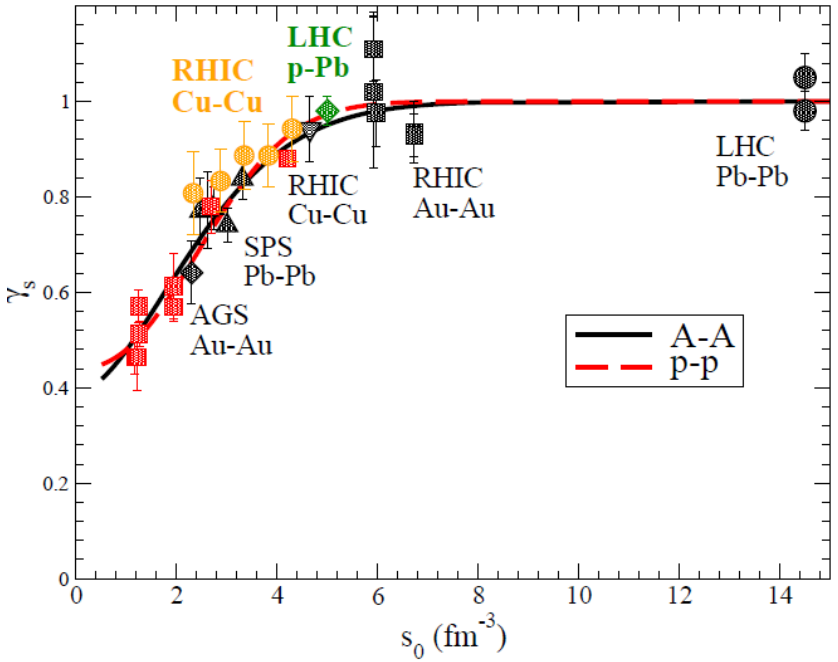

$$R_p = 0.8 \text{ fm} \qquad R_A = 1.25A^{1/3} \qquad R_T = R_p(0.5\bar{N}_{\text{part}})^{1/3}$$

B. Abelev et al. (ALICE Coll.), Phys. Rev. Lett. 110 (2013) 032301

More refined analysis – in particular for high multiplicity pp events

Glauber model references: gereral [4], Alice [1] Transverse area [3, 2], wood saxon for deformed nuclei [5]

AA

[1] B. Abelev *et al.* [ALICE Collaboration], Phys. Rev. C **88** (2013) no.4, 044909 doi:10.1103/PhysRevC.88.044909 [arXiv:1301.4361 [nucl-ex]].

[2] J. Adam *et al.* [ALICE Collaboration], Phys. Rev. C **93** (2016) no.3, 034916 doi:10.1103/PhysRevC.93.034916 [arXiv:1507.06194 [nucl-ex]].

[3] B. Alver *et al.*, Phys. Rev. C **77** (2008) 014906 doi:10.1103/PhysRevC.77.014906 [arXiv:0711.3724 [nucl-ex]].

[4] M. L. Miller, K. Reygers, S. J. Sanders and P. Steinberg, Ann. Rev. Nucl. Part. Sci. **57** (2007) 205 doi:10.1146/annurev.nucl.57.090506.123020 [nucl-ex/0701025].

[5] P. Filip, R. Lednicky, H. Masui and N. Xu, Phys. Rev. C **80** (2009) 054903. doi:10.1103/PhysRevC.80.054903

Pb-Pb, $\sqrt{s_{NN}} = 2.76TeV$

Au–Au, $\sqrt{s_{NN}} = 200GeV$

Cu–Cu, $\sqrt{s_{NN}} = 200GeV$

Pb-Pb, $\sqrt{s_{NN}} = 2.76TeV$

Bin	V0M	b (fm)	N_part	$\langle S_T^{V0M} \rangle$	$\langle S_T^b \rangle$	$\langle S_T^{Npart} \rangle$	$\langle N_{part}^{V0M} \rangle$
0.0-0.1	-2-14020	0.03-4.89	-2-306	110.7 ± 0.0	111.1 ± 0.0	111.5 ± 0.0	356.4 ± 0.1
0.1-0.2	14020-9368	4.89-6.93	306-222	90.0 ± 0.0	90.1 ± 0.0	90.3 ± 0.0	261.1 ± 0.0
0.2-0.4	9368-3834	6.93-9.81	222-106	65.6 ± 0.0	65.5 ± 0.0	65.7 ± 0.0	158.0 ± 0.0
0.4-0.6	3834-1244	9.81-12.03	106-40	41.2 ± 0.0	40.9 ± 0.0	41.2 ± 0.0	69.3 ± 0.0
0.6-0.8	1244-264	12.03-13.89	40-10	21.4 ± 0.0	21.3 ± 0.0	21.8 ± 0.0	22.6 ± 0.0
0.8-0.9	264-84	13.89-14.91	10-4	7.9 ± 0.0	9.0 ± 0.0	8.5 ± 0.0	6.7 ± 0.0
0.9-1.0	84-8	14.91-16.89	4-2	2.1 ± 0.0	3.7 ± 0.0	2.9 ± 0.0	2.8 ± 0.0

$\sigma_{NN} = 64$ mb

A = 208

RA=6.59

Glauber Montecarlo - ALICE

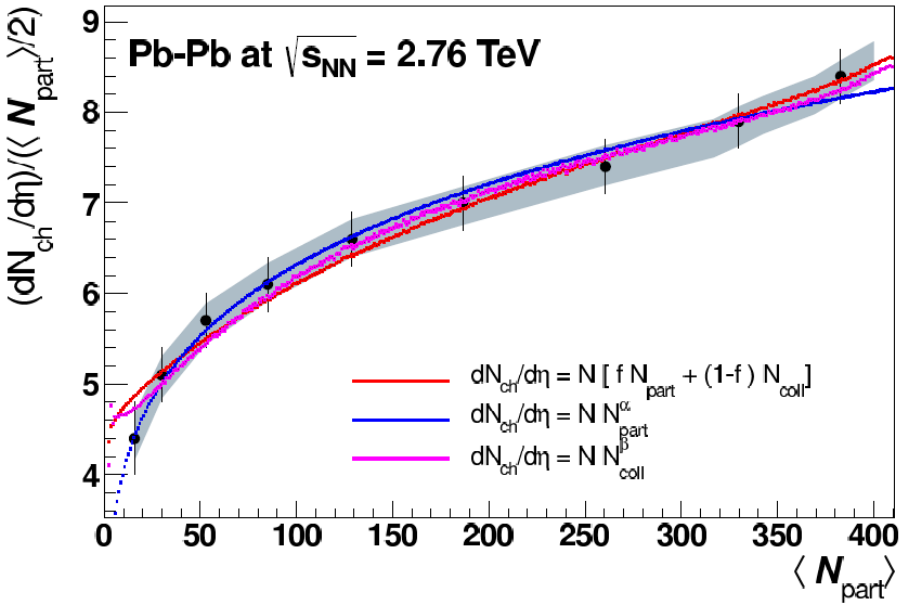

Fig. 11: (Color online) Centrality dependence of $dN_{ch}/d\eta$ per participant pair as a function of N_{part}, measured in the Pb–Pb data at $\sqrt{s_{NN}} = 2.76$ TeV fitted with various parametrizations of N_{part} and N_{coll}, calculated with the Glauber model. The fit parameters are given in the figure.

pp

Note that $\dfrac{1.5A^x}{\pi R_x^2}\left(\dfrac{dN_{ch}}{dy}\right)^x_{y=0}$

$$Q_s^2 = \frac{1}{A}\left(\frac{dN_h}{dy}\right)_{y=0}$$

- color glass condensate: parton density in transverse plane

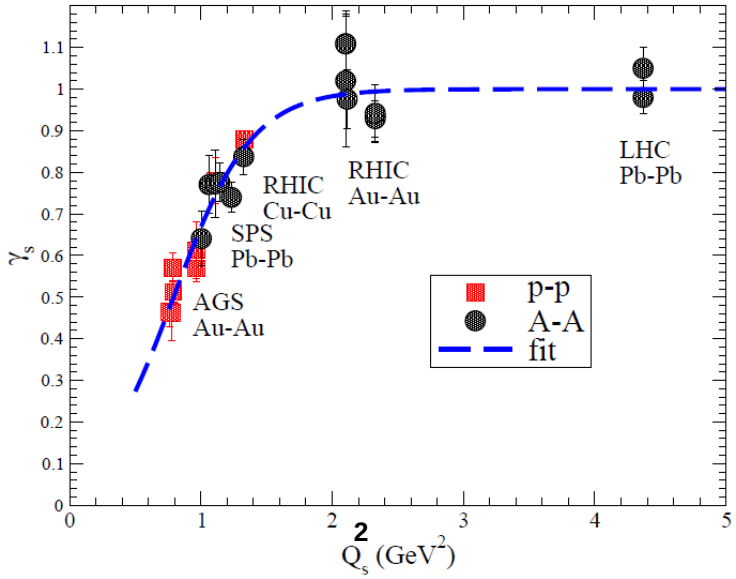

Fluctuactions in the effective transverse area ：

L.McLerran,M.Praszalowicz,B.Schenke 1306.2350

A.Badak,B.Schenke,P.Tribedy,R.Venugopal 1304.3403

L.McLerran,P.Tribedy 1508.03292

L.McLerran,M.Praszalowicz 1507.0597

C. Marquet, G. Soyez, B.-W. Xiao, On the probability distribution of the stochastic saturation scale in QCD, Phys. Lett. B639 (2006) 635–641. arXiv:hep-ph/0606233, doi:10.1016/j.physletb.2006.07.022.

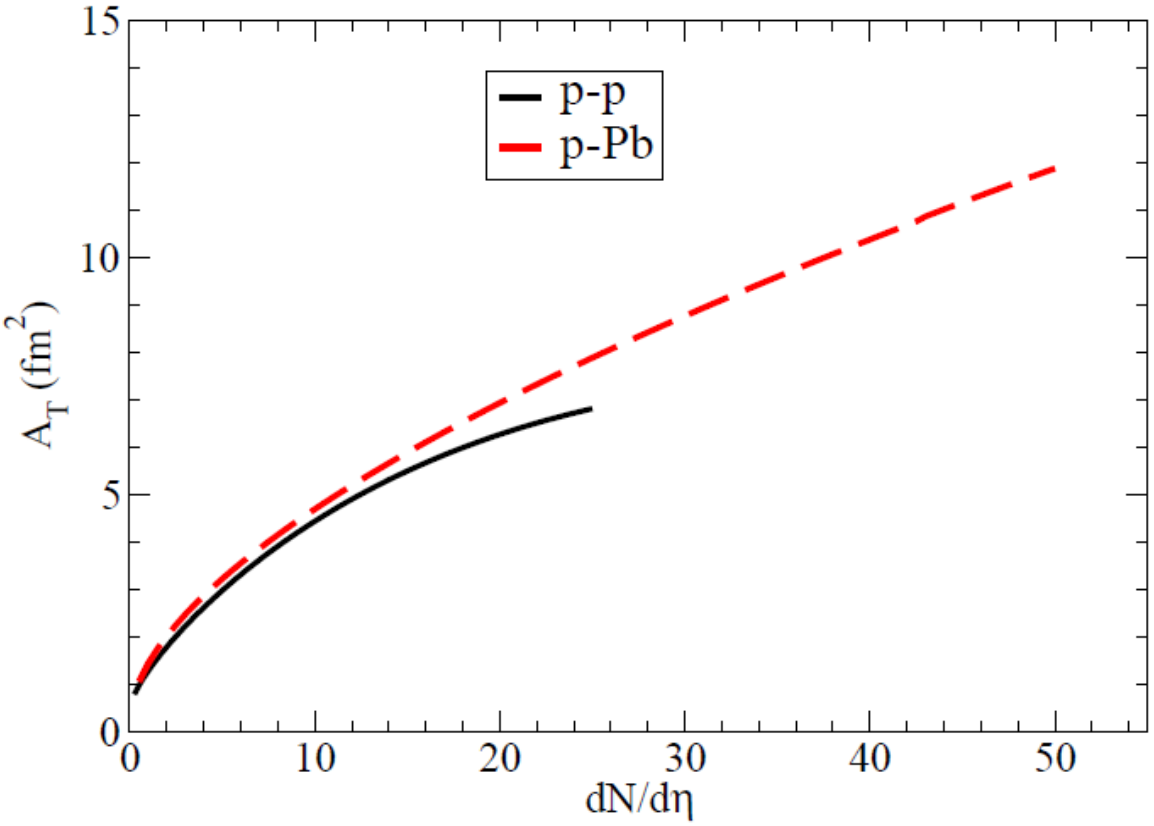

Different species

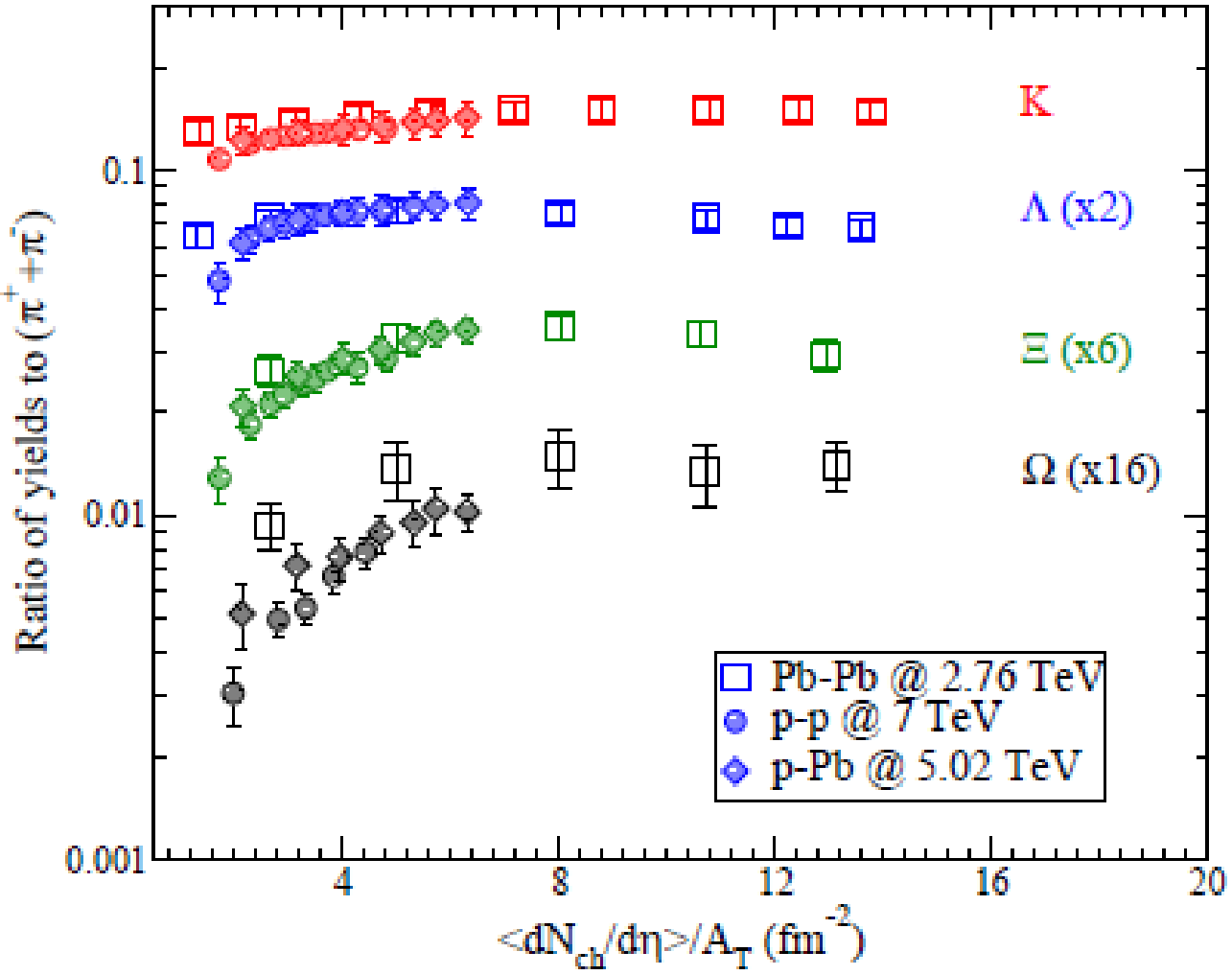

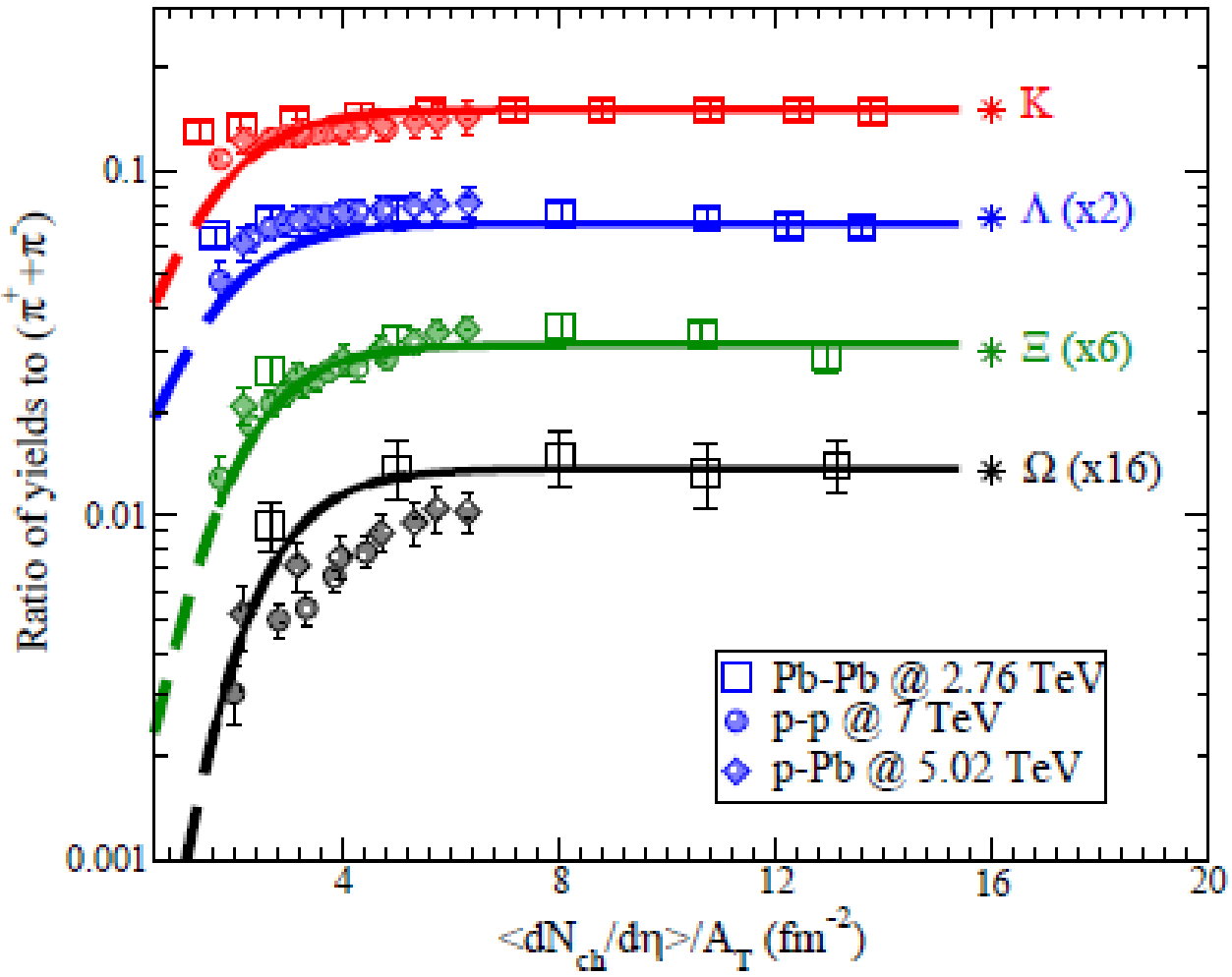
Ratio of yields to ($\pi^+ + \pi^-$)
0.1
0.01
0.001
4
8
12
16
20
$\langle dN_{ch}/d\eta \rangle / A_T$ (fm^{-2})
* K
* Λ (x2)
* Ξ (x6)
* Ω (x16)
Pb-Pb @ 2.76 TeV
p-p @ 7 TeV
p-Pb @ 5.02 TeV

Conclusions

- Universal behavior of strangeness production in pp, pA, AA

Why? 1601.01454
1603.06529
P.C.,S.Plumari,H.Satz

- Dynamical variable $= \frac{1}{A}\left(\frac{dN_h}{dy}\right)_{y=0}$
- Fluctuactions in the effective transverse area
- For event with higher multiplicity – some difference between pA and pp
- Relation with deconfinement – thermal variables

H.Satz's talk at SQM 2017

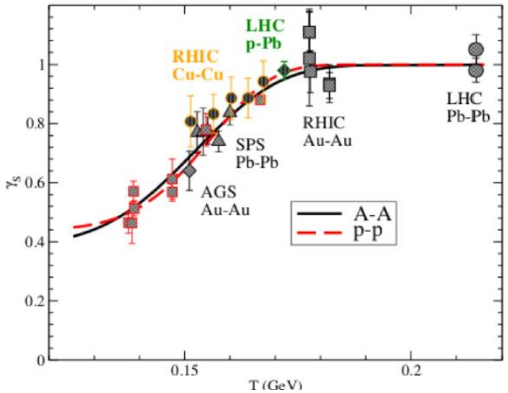

SM 1

1. Thermal Hadron Production

what is "thermal"? J.Cleymans lectures 1+2

- equal *a priori* probabilities for all states in accord with given overall average energy $\Rightarrow$ temperature T;

- partition function of ideal resonance gas

$$\ln Z(T) = V \sum_i \frac{d_i}{(2\pi)^3} \phi(m_i, T)$$

Boltzmann factor $\phi(m_i, T) = 4\pi m_i^2 T K_2(m_i/T) \sim \epsilon^{-m_i/T}$;

- relative abundances $\frac{N_i}{N_j} = \frac{d_i \phi(m_i, T)}{d_j \phi(m_j, T)} \sim \epsilon^{-(m_i - m_j)/T}$

predicted in terms of temperature T

In the grand-canonical formulation of the statistical model, the mean hadron multiplicities are defined as

$$\langle N_i \rangle = (2J_i + 1)\frac{V}{(2\pi)^3}\int \mathrm{d}^3 p \, \frac{1}{\gamma_s^{-s_i}\exp[(E_i - \mu \cdot \mathbf{q_i})/T_{\mathrm{ch}}] \pm 1}$$

Fireball volume

Strangeness suppression

Number of s or anti-s

chemical potentials

Ch**emi**cal Freeze –out Temperature = hadronic abundances get frozen

baryon number B_i, third component of the isospin I_{3i}, strangeness S_i, and charmness C_i, the chemical potential is $\mu_i = \mu_b B_i + \mu_{I_3} I_{3i} + \mu_S S_i + \mu_C C_i$. The chemical potentials related to baryon number (μ_b), isospin (μ_{I_3}), strangeness (μ_S) and charm (μ_C) ensure the conservation (on average) of the respective quantum numbers: i) baryon number: $V\sum_i n_i B_i = N_B$; ii) isospin: $V\sum_i n_i I_{3i} = I_3^{tot}$; iii) strangeness: $V\sum_i n_i S_i = 0$; iv) charm: $V\sum_i n_i C_i = 0$.

- massive colorless clusters distributed over rapidities,
  each decays statistically
- mass and charge distributions of clusters again statistically
  $\Rightarrow$ equivalent global cluster
- $V = \Sigma\, V_i$, $Q = \Sigma\, Q_i$; large enough for thermodynamics

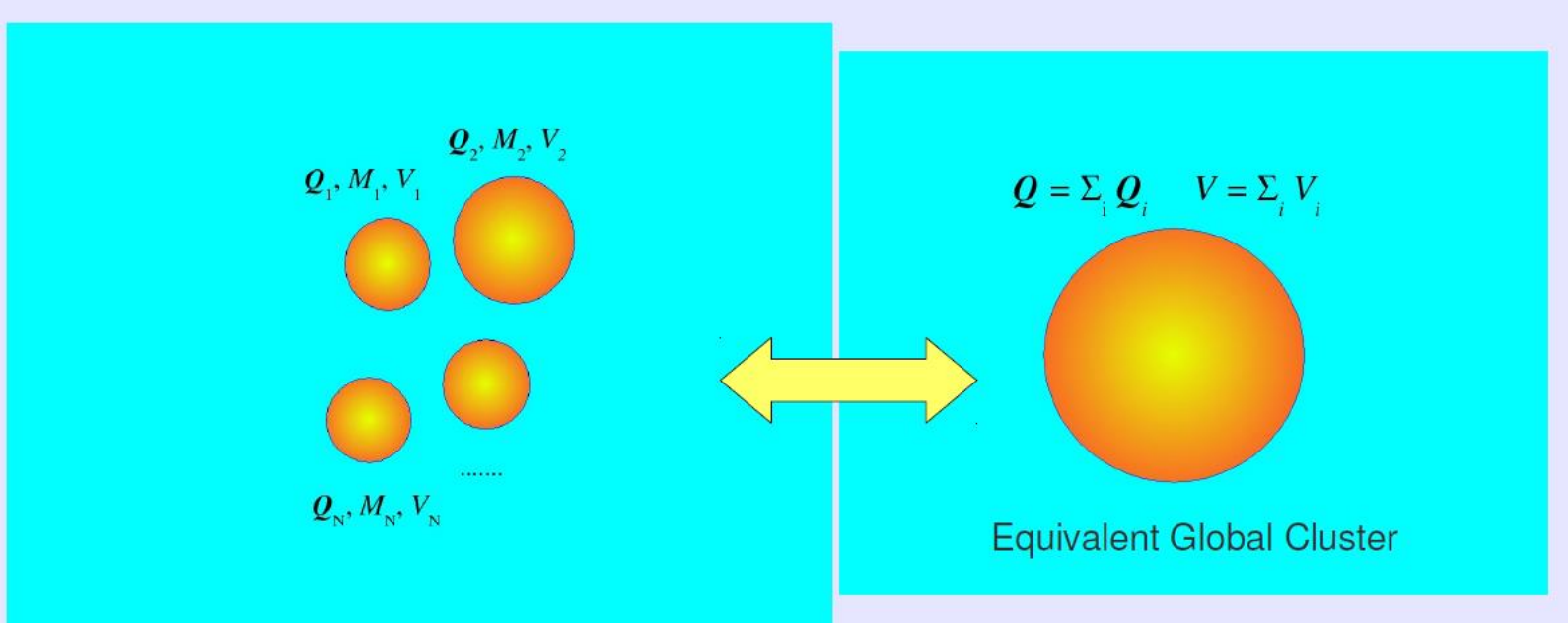

First, a primary hadron yield $\langle n_j \rangle^{\text{primary}}$ is calculated using previous equations.

As a second step, all resonances in the gas which are unstable against strong decays are allowed to decay into lighter stable hadrons, using appropriate branching ratios (B) for the decay k → j published by the PDG. The abundances in the final state are thus determined by

$$\langle n_j \rangle = \langle n_j \rangle^{\text{primary}} + \sum \langle n_k \rangle BR(k \to j).$$

$$T, V, \gamma_s, \mu_b$$

Fit statistical hadronization at LHC

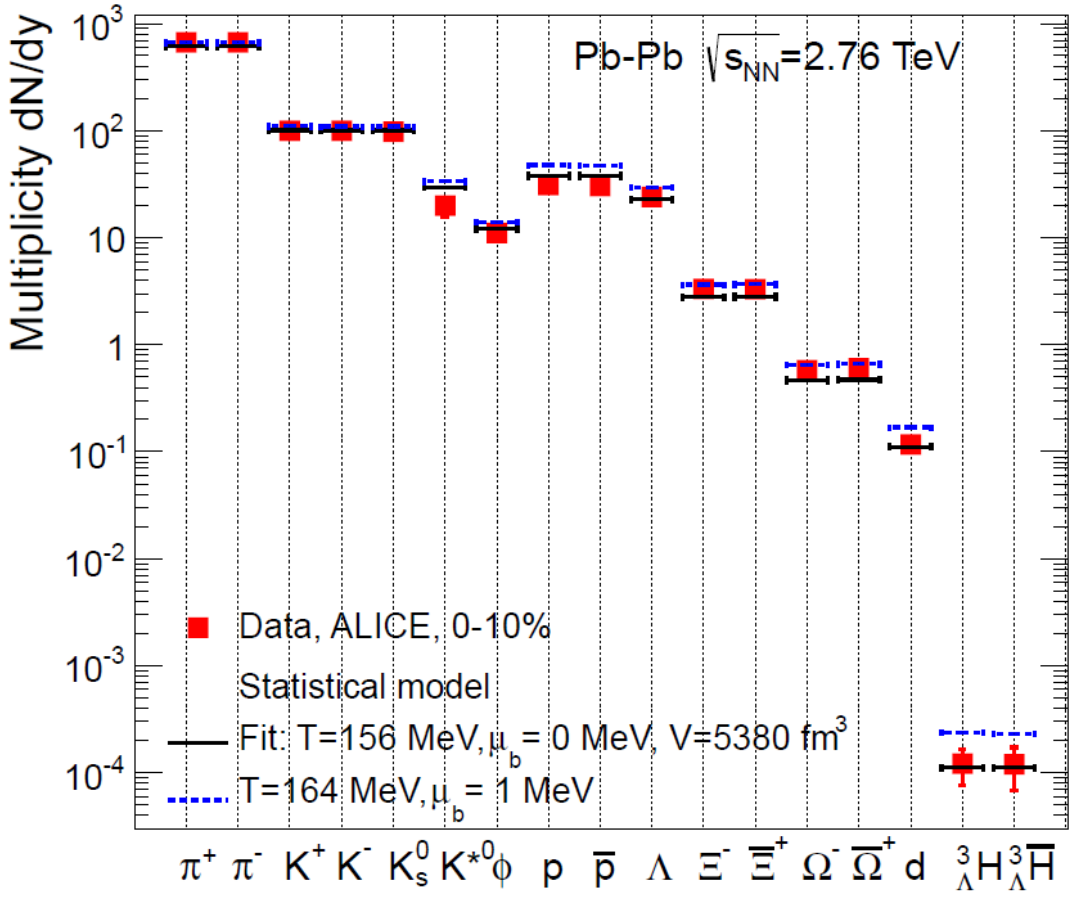

J Stachel, A Andronic, P Braun-Munzinger, K Redlich arxiv:1311.4662

Canonical suppression SM 2

In elementary collisions, the clusters at rapidities sufficiently far apart are causally disconnected, so that they cannot exchange information. Hence strangeness must be conserved locally

Correlation volume for strangeness

Volume of the causally connected cluster

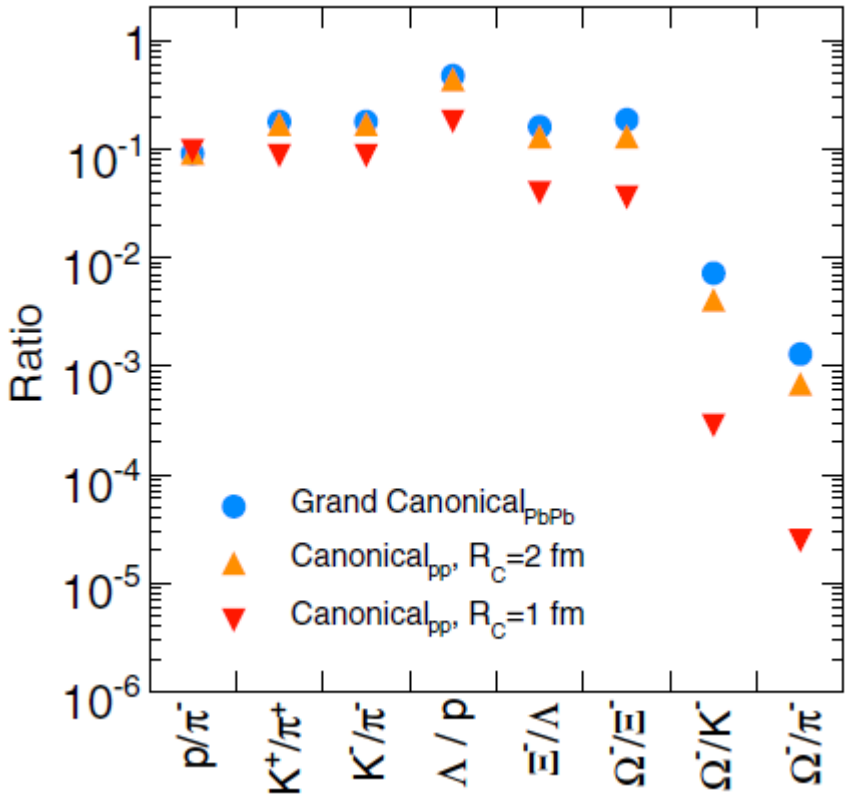

Statistical Thermodynamics in Relativistic Particle and Ion Physics: Canonical or Grand Canonical?

R. Hagedorn and K. Redlich Z. Phys. C - Particles and Fields 27, 541-551 (1985)

Canonical aspects of strangeness enhancement

A. Tounsia, A. Mischkeb and K. Redlich hep-ph/0209284

I Kraus, J Cleymans, H Oeschler and K Redlich

J. Phys. G: Nucl. Part. Phys. **37** (2010) 094021

Canonical suppression

Statistical Thermodynamics in Relativistic Particle and Ion Physics: Canonical or Grand Canonical?
R. Hagedorn and K. Redlich

Canonical aspects of strangeness enhancement
A. Tounsia, A. Mischkeb and K. Redlich hep-ph/0209284

$$\langle N_i \rangle = (2J_i+1)\frac{V}{(2\pi)^3}\int \mathrm{d}^3p\,\frac{1}{\gamma_s^{-s_i}\exp[(E_i-\mu\cdot\mathbf{q_i})/T_{\mathrm{ch}}]\pm 1}$$

The nature of V in elementary collisions is quite different from that in nuclear collisions and this can in effect lead to different behavior for strangeness production .

τ_q ,specifies a boost-invariant proper time at which local volume elements experience the transition from an initial state of frozen virtual partons to the partons which will eventually form hadrons

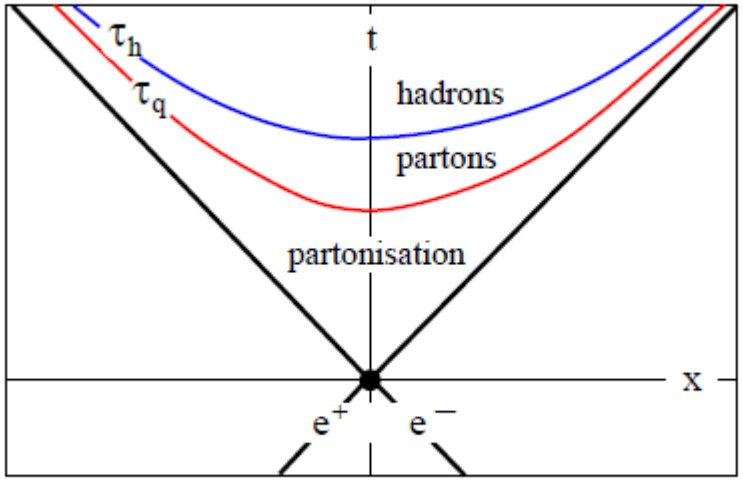

$$\sigma x_q = 2\sqrt{m_q^2+k_T^2},$$

$$k_T = \sqrt{\pi\sigma/2},$$

$$x_q \simeq \sqrt{\frac{2\pi}{\sigma}} \simeq 1\ \mathrm{fm},$$

arXiv:1310.6932
P.C. and H.Satz Causality Constraints on Hadron Production In High Energy Collisions

bubble of partonic medium of proper time τ
with $\tau_q < \tau < \tau_h$: fireball;
fireballs at different spatial
rapidities η

$t = \tau \cosh \eta, \quad x = \tau \sinh \eta,$

with transition lines

$t^2 - x^2 = \tau^2$

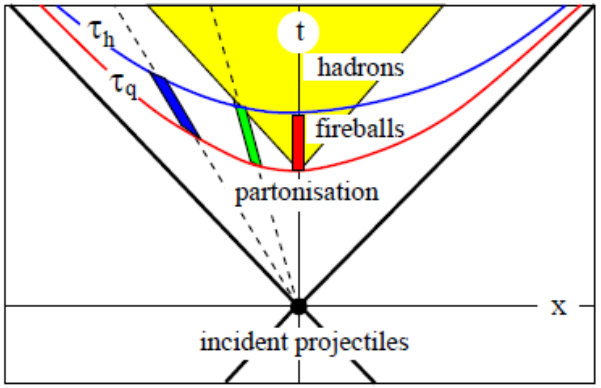

red fireball ($\eta = 0$) - causality region yellow
green fireball ($\eta = \eta_d$) - one common x-t point with red
blue fireball ($\eta > \eta_d$) - outside causality region of red

for $\eta > \eta_d$, with $\tanh \eta_d = (\tau_h^2 - \tau_q^2)/(\tau_h^2 + \tau_q^2)$

forward and backward fireballs are out of communication
with central fireball

examples:

$\tau_q = 1$ fm, $\tau_h = 2$ fm $\rightarrow \eta_d = 0.7$

$\tau_q = 1$ fm, $\tau_h = 7$ fm $\rightarrow \eta_d = 2$

at RHIC and LHC, hadronisation occurs through causally disjoint fireballs

so far, have neglected spatial size:
what is the size of a fireball?
define through causal connectivity

require: the most separate points can still communicate

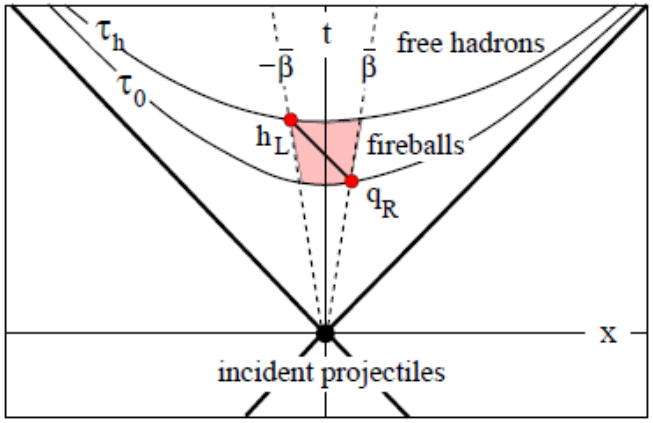

spatial diameter d of fireball in cms at hadronisation time

$$d = \sqrt{\frac{\tau_h}{\tau_q}}(\tau_h - \tau_q)$$

causal connection (and hence correlations) for hadron production at large rapidity intervals; ⇒ means that any correlations originated in the earlier partonisation stage.

examples for different hadronisation times:

τ_h [fm]	β	η	$r = d/2$ [fm]
2	0.33	0.35	0.7
3	0.50	0.55	1.7
4	0.60	0.69	3.0
5	0.67	0.81	4.5

We now assume complete boost invariance: the collision leads to the production of identical fireballs at all rapidities, with identical formation and hadronisation times τ_q, τ_h in their respective rest frames. To study the causal connection of fireballs moving at dif-

denote average cms velocity of of central fireball by $\bar{\beta}_0 = 0$ can then partition production region into successive causally disjoint fireballs, of velocities

$$\bar{\beta}_n = \frac{\tau_h^{2n} - \tau_q^{2n}}{\tau_h^{2n} + \tau_q^{2n}}$$

$$n = 0, 1, 2, ...$$

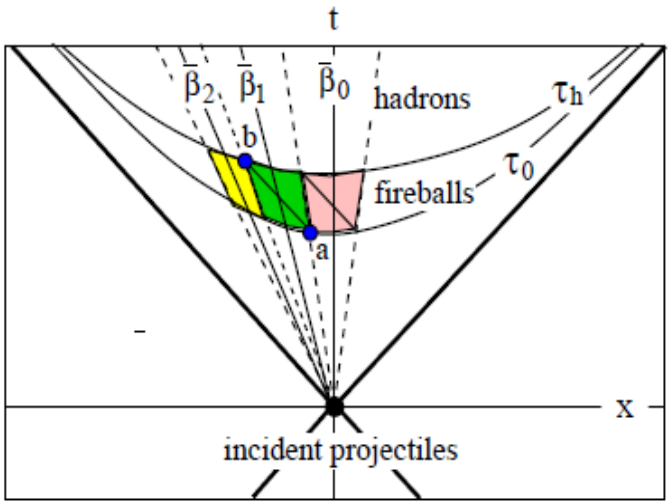

one fireball - require that the spatially right-most point q_R at formation can send a signal to the spatially left-most point h_L at hadronisation; i.e., we require that the most separate points of the fireball can still communicate.

τ_h [fm]	$\bar{\beta}$	η	r [fm]
2	0.33	0.35	0.7
3	0.50	0.55	1.7
4	0.60	0.69	3.0
5	0.67	0.81	4.5

Table 1: Velocity (β) and rapidity (η) limits of a fireball at rest in the center of mass, and its proper hadronisatin radius r, as given by eqs. 9 and 10, for a formation time $\tau_q = 1$ fm and different hadronisation times τ_h.

Hadronization

$$\langle N_i \rangle = (2J_i + 1)\frac{V}{(2\pi)^3}\int \mathrm{d}^3p\,\frac{1}{\gamma_s^{-s_i}\exp[(E_i - \mu\cdot\mathbf{q_i})/T_{\mathrm{ch}}] \pm 1}$$

V = volume of the equivalent global cluster

In elementary collisions, the clusters at rapidities sufficiently far apart are, as we have seen, causally disconnected, so that they cannot exchange information. Hence strangeness must be conserved locally; in pp collisions, for example, each cluster must have strangeness zero.

In high energy nuclear collisions the equivalent global cluster consists of the different clusters from the different nucleon-nucleon interactions at a common rapidity. At mid-rapiditiy, for example, we thus have the sum of the superimposed mid-rapidity clusters from the different nucleon-nucleon collisions, and these are all causally connected, allowing strangeness exchange and conservation between the different clusters

SM 3 Fluctuactions in the saturation scale -CGC

The Interaction Area a computation based on an impact parameter description of pp collisions, combined with an underlying description of particle production based on the theory of the Color Glass Condensate.

- the interaction radius is approximately a linear function of $(dN/dy)^{1/3}$ for dN/dy less than some critical value

The saturation of the radius R as a function of $(dN/dy)^{1/3}$ can be understood in the following way. For smaller multiplicities, the number of produced particles is proportional to the interaction volume $\propto R^3$.

Once maximal overlap ($b = 0$ fm) is achieved, higher multiplicities can only be reached by certain color charge fluctuations, which do not increase the size of the system. This argument also holds for pA collisions, where $b = 0$ fm corresponds to an overlap of the proton with the densest region of the nucleus.

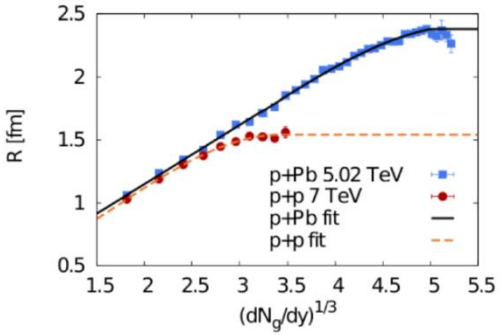

Different Sources of Fluctuations in CGC

- the distribution of the saturation scale in the co-ordinate space transverse to collision direction at a given energy, $Q_S^2(\mathbf{s}_\perp)$.

- The second source of the fluctuations in the IP-Glasma model is of geometric origin. The gluon fields produced after the collision of two protons are obtained in terms of the gluon fields of the two colliding protons. The resultant field after the collision vanishes in the region where the fields of the two protons do not overlap. Therefore an additional source of stochasticity is introduced by the fluctuations in the overlap area of the two protons due to fluctuation in the impact parameter of the collision. The

- intrinsic fluctuations of the saturation momentum

Gaussian in $\ln(Q_S^2(Y))$ and the correction to the Gaussian fluctuations is negligible at large Y.

C. Marquet, G. Soyez, B.-W. Xiao, On the probability distribution of the stochastic saturation scale in QCD, Phys. Lett. B639 (2006) 635–641. arXiv:hep-ph/0606233, doi:10.1016/j.physletb.2006.07.022.

SM 4

Glauber Montecarlo - ALICE

$$\rho(r) = \rho_0 \frac{1 + w(r/R)^2}{1 + \exp\left(\frac{r-R}{a}\right)}$$

$R = (6.62 \pm 0.06)$ fm is the radius parameter of the ^{208}Pb nucleus and $a = (0.546 \pm 0.010)$ fm is the skin thickness of the nucleus, which indicates how quickly the nuclear density falls off near the edge of the nucleus. w=0 for Pb

$\sqrt{s_{\mathrm{NN}}} = 2.76$ TeV, we use $\sigma_{\mathrm{NN}}^{\mathrm{inel}} = (64 \pm 5)$ mb,

Centrality determination of Pb–Pb collisions at $\sqrt{s_{\mathrm{NN}}}$= 2.76 TeV with ALICE

ALICE Collaboration *

SM 4

Glauber Montecarlo - ALICE

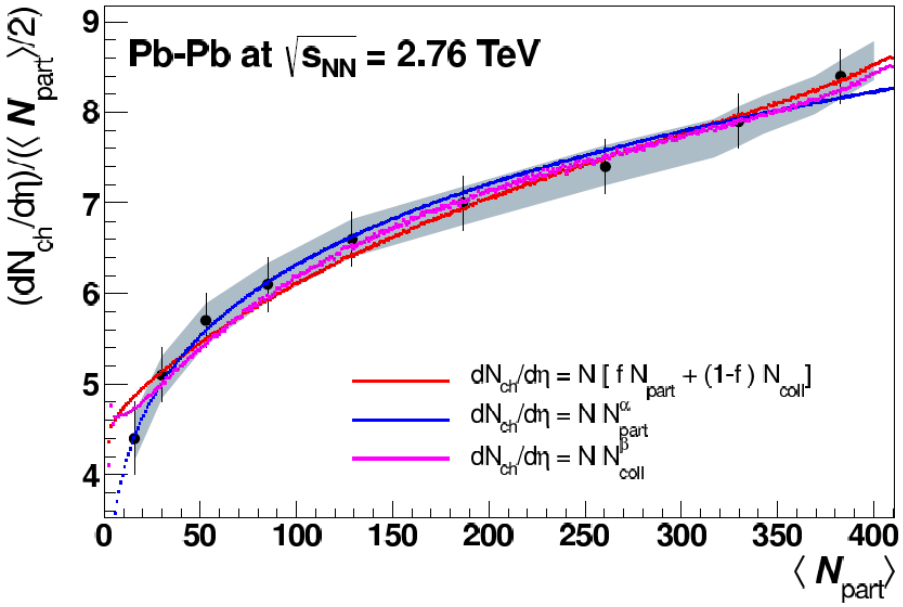

Fig. 11: (Color online) Centrality dependence of $dN_{ch}/d\eta$ per participant pair as a function of N_{part}, measured in the Pb–Pb data at $\sqrt{s_{NN}} = 2.76$ TeV fitted with various parametrizations of N_{part} and N_{coll}, calculated with the Glauber model. The fit parameters are given in the figure. Data are from [35].